

# Quantifying Gyrotropy in Magnetic Reconnection

M. Swisdak\*

A new scalar measure of the gyrotropy of a pressure tensor is defined. Previously suggested measures are shown to be incomplete by means of examples for which they give unphysical results. To demonstrate its usefulness as an indicator of magnetic topology, the new measure is calculated for electron data taken from numerical simulations of magnetic reconnection, shown to peak at separatrices and X-points, and compared to the other measures. The new diagnostic has potential uses in analyzing spacecraft observations and so a method for calculating it from measurements performed in an arbitrary coordinate system is derived.

## I. INTRODUCTION

The term magnetic reconnection, as commonly understood, refers to a process whereby the energy of the embedded field is transferred to the surrounding plasma via bulk acceleration and Ohmic dissipation. While frequently associated with changes in the topology of the magnetic field, precisely defining where and how reconnection occurs is a surprisingly subtle task [1].

In what are known as 2.5D geometries, where variations in one direction are suppressed, the coupling of the reduced dimensionality with the divergence-free nature of the magnetic field allows field lines to be completely characterized as contours of a scalar function,  $\psi$ . ( $\psi$  is equivalent to the component of the magnetic vector potential in the invariant direction.) Saddle points of  $\psi$ , known as X-points, mark locations of both topological change and magnetic reconnection. In fully three-dimensional systems, field lines can no longer be described by a single function and characterizing reconnection becomes significantly more difficult. Finding the locations where magnetic reconnection occurs is non-trivial, even in numerical simulations [2–4].

Yet simulations have the luxury of a synoptic view with, in principle, access to the complete description of the plasma at any point in the domain. Spacecraft observations, in contrast, must make due with a limited set of measurements available from, at most, a few locations. The topological identification of reconnection sites is non-local in nature and hence extremely difficult to implement with these restrictions. Determinations must instead be based on local measurements of the electromagnetic fields and particles.

Due to their small Larmor radii and brief gyroperiods, electrons are closely tied to the magnetic field, much more so than the heavier ions. By streaming for long distances along field lines they efficiently probe magnetic structure and so locations of topological interest, such as reconnection sites, should leave signatures in electron measurements. [5] identified one such signature by noting that, because of finite Larmor radius effects, the guiding center approximation breaks down near an X-point. One

consequence is that reconnection, at least in 2.5D, requires an asymmetry (specifically, non-gyrotropy) in the electron pressure tensor there. Spacecraft measurements of electron distribution functions can hence be used as a proxy for topology. In this paper we present a diagnostic quantifying the size of departures from gyrotropy and demonstrate, through numerical simulations, that it faithfully maps regions associated with magnetic reconnection.

## II. MEASURING GYROTROPY

Given a distribution function  $f(\mathbf{x}, \mathbf{v})$  that describes the density of particles with mass  $m$  in a phase space defined by position ( $\mathbf{x}$ ) and velocity ( $\mathbf{v}$ ), the pressure  $\mathbb{P}$  can be defined as

$$\mathbb{P} = m \int \mathbf{w} \mathbf{w} f d^3 \mathbf{v}, \quad (1)$$

where  $\mathbf{w} = \mathbf{v} - \bar{\mathbf{v}}$  is the velocity relative to the mean flow  $\bar{\mathbf{v}}$ . While  $\mathbb{P}$  is, in general, a tensor with six independent components, it can be characterized by a single scalar when  $f$  is spherically symmetric (e.g., a Maxwellian). A magnetic field, by imposing a preferred direction, can produce a cylindrically symmetric, or gyrotropic, distribution. In this case the pressure tensor takes the form

$$\mathbb{P} = P_{\parallel} \hat{\mathbf{b}} \hat{\mathbf{b}} + P_{\perp} (\mathbb{I} - \hat{\mathbf{b}} \hat{\mathbf{b}}), \quad (2)$$

where  $\hat{\mathbf{b}} = |\mathbf{B}|/B$  is a unit vector in the direction of the magnetic field,  $P_{\parallel}$  and  $P_{\perp}$  are scalars, and  $\mathbb{I}$  is the unit tensor. In the equivalent matrix formulation,

$$\mathbb{P} = \begin{pmatrix} P_{\parallel} & 0 & 0 \\ 0 & P_{\perp} & 0 \\ 0 & 0 & P_{\perp} \end{pmatrix}. \quad (3)$$

Observationally, pressure tensors are never completely gyrotropic because of the presence of non-zero off-diagonal components, although these are often much smaller than the diagonal terms. Since departures from gyrotropy are expected to be associated with locations of magnetic reconnection, a quantitative measure of this smallness would be useful.

With this goal in mind, [6] proposed a measure, dubbed the agyrotropy and denoted  $A\mathcal{O}_e$ , that characterizes a

\* swisdak@umd.edu

distribution function's weighted average of dispersions of velocities perpendicular to the local field direction (see Appendix A of their paper for a full description). It varies between 0 and 2 with the minimum supposedly corresponding to gyrotropic distributions. However, as demonstrated below, there exist agyrotropic pressure tensors for which  $A\varnothing_e = 0$ .

[7] proposed another measure, denoted  $D_{ng}$  and named non-gyrotropy. It is proportional to the root-mean-square of the off-diagonal elements of the pressure tensor normalized by the local thermal energy. As with the agyrotropy,  $D_{ng} = 0$  for a gyrotropic distribution but, as also shown below, there exist pressure tensors with maximal departures from gyrotropy for which  $D_{ng}$  is arbitrarily close to 0.

A brief mathematical digression is necessary in order to justify a better measure. Because pressure tensors originate as moments of distribution functions, their matrix representations must satisfy certain constraints. Specifically, a physically meaningful pressure tensor is a real  $3 \times 3$  symmetric matrix (i.e.,  $P_{ij} = P_{ji}$ ) with non-negative eigenvalues. Matrices possessing these properties, including all pressure tensors, are called symmetric positive semi-definite. If all of the eigenvalues are positive the matrix is positive definite. (That the eigenvalues of a pressure tensor must be non-negative follows from the requirement that after diagonalization, which is always possible for a real symmetric matrix, the matrix elements are both the eigenvalues and the components of the pressure along the basis vectors of the rotated frame. For physical distributions the latter, and hence the former, must be greater than or equal to zero.)

Defining a scalar measure of gyrotropy requires a result from the theory of symmetric positive semi-definite matrices. It can be shown [8] that a matrix is positive semi-definite if and only if all principal minors – the determinants of every submatrix arising from deleting the same set of rows and columns – are non-negative. (If zero eigenvalues are excluded, so that the matrix is positive definite, Sylvester's criterion applies [8]. In this case, a necessary and sufficient condition is that the leading principal minors, i.e., the determinants of all upper-left submatrices, be positive.)

A pressure tensor with gyrotropic diagonal, but non-zero off-diagonal, entries can be written as

$$\mathbb{P} = \begin{pmatrix} P_{\parallel} & P_{12} & P_{13} \\ P_{12} & P_{\perp} & P_{23} \\ P_{13} & P_{23} & P_{\perp} \end{pmatrix}. \quad (4)$$

In this representation one of the coordinate axes points in the direction of the local magnetic field and the others are oriented such that the final two components of the diagonal of  $\mathbb{P}$  are equal. (That this is always possible is demonstrated in the Appendix.) Since  $\mathbb{P}$  is positive semi-definite the result discussed above implies the inequalities

$$P_{12}^2 \leq P_{\parallel} P_{\perp} \quad P_{13}^2 \leq P_{\parallel} P_{\perp} \quad P_{23}^2 \leq P_{\perp}^2. \quad (5)$$

The converse does not hold: satisfaction of these inequalities does not guarantee that  $\mathbb{P}$  is positive semi-definite.

Adding the inequalities implies a natural definition for a measure of gyrotropy:

$$Q = \frac{P_{12}^2 + P_{13}^2 + P_{23}^2}{P_{\perp}^2 + 2P_{\perp}P_{\parallel}}. \quad (6)$$

For gyrotropic tensors  $Q = 0$ , while for maximal departures from gyrotropy  $Q = 1$ . Evaluating  $Q$  from equation 6 requires  $\mathbb{P}$  to be in the form given by equation 4 even though, in general,  $\mathbb{P}$  is measured in an arbitrary coordinate system. While it is always possible to rotate  $\mathbb{P}$  into a frame in which it has the form of equation 4, the Appendix demonstrates how to calculate  $Q$  without such a transformation by using tensor invariants.

The theory of positive semi-definite matrices provides a firm mathematical basis for the definition of  $Q$ . With it in mind, it is possible to construct pressure tensors for which other proposed measures give physically unreasonable results. Consider a system with a pressure tensor, of the type shown in equation 4, given by

$$\mathbb{P} = \begin{pmatrix} 1 & 1/2 & 0 \\ 1/2 & 1 & 0 \\ 0 & 0 & 1 \end{pmatrix}. \quad (7)$$

Since  $\mathbb{P}$  has eigenvalues of  $1/2$ ,  $1$ , and  $3/2$ , it is positive semi-definite and hence physically valid. Yet, despite the off-diagonal elements that make it clearly not gyrotropic,

$$A\varnothing_e = 0. \quad (8)$$

For reference,  $\sqrt{Q} = \sqrt{3}/6$  and  $D_{ng} = \sqrt{2}/3$  in this case. (The other gyrotropy measures considered here scale as ratios of first powers of pressure components while  $Q$  scales quadratically. The subsequent discussion, where necessary to ensure an unbiased comparison, uses  $\sqrt{Q}$ .)

In fact  $A\varnothing_e = 0$  for any positive semi-definite  $\mathbb{P}$  in the form of equation 4 with  $P_{23} = 0$ , irrespective of the other off-diagonal components. This occurs because, by construction,  $A\varnothing_e$  only measures departures from symmetry in the plane perpendicular to the magnetic field axis. However, as equation 7 demonstrates, there are other ways in which pressure tensors can depart from gyrotropy. The vanishing of  $A\varnothing_e$  for such cases indicates that it does not fully describe a pressure tensor's gyrotropy.

The nongyrotropy measure proposed by [7] is defined as

$$D_{ng} = \frac{\sqrt{8(P_{12}^2 + P_{13}^2 + P_{23}^2)}}{P_{\parallel} + 2P_{\perp}}. \quad (9)$$

The most significant difference between it and  $\sqrt{Q}$  occurs in the normalization, which for  $D_{ng}$  is to the thermal energy,  $P_{\perp} + P_{\parallel}/2$ . As with the other measures,  $D_{ng} = 0$  for gyrotropic tensors. The maximum value of  $D_{ng}$  varies with  $P_{\parallel}/P_{\perp}$ , which is not the case for either  $Q$  or  $A\varnothing_e$ . Its global maximum of  $\sqrt{8/3}$  occurs when  $P_{\parallel} = P_{\perp}$ .

The implications of this variation become apparent through consideration of the pressure tensor

$$\mathbb{P} = \begin{pmatrix} x & \sqrt{x} & \sqrt{x} \\ \sqrt{x} & 1 & 1 \\ \sqrt{x} & 1 & 1 \end{pmatrix} \quad (10)$$

with  $x \geq 0$ . Eigenvalues of 0, 0, and  $x + 2$  mean that  $\mathbb{P}$  is positive semi-definite. The gyrotropy measures are

$$D_{ng} = \frac{\sqrt{8(2x+1)}}{x+2}, \quad \sqrt{Q} = 1, \quad \text{and } A\varnothing_e = 2. \quad (11)$$

This pressure tensor is maximally non-gyrotropic for any value of  $x$  because any perturbation that increases the off-diagonal components will drive one of the eigenvalues negative. Any measure of the gyrotropy for this  $\mathbb{P}$  should thus be independent of  $x$  and should take its maximal value. Yet  $D_{ng}$  varies with  $x$ . This behavior does not depend on  $\mathbb{P}$  having zero eigenvalues, although such a case is the simplest to analyze. Similar pressure tensors exist that both have three positive eigenvalues exist and approach arbitrarily close to maximal non-gyrotropy yet for which  $D_{ng}$  varies in a manner similar to Equation 11.

The examples of equations 7 and 10 are instances where the deficiencies of  $A\varnothing_e$  and  $D_{ng}$  in quantifying gyrotropy are particularly clear. To a lesser or greater degree similar issues will be present for other pressure tensors, although in any specific example it may be difficult to tease out the degree to which the gyrotropy is mischaracterized.

### III. SIMULATIONS

While the arguments of the previous section suggest that  $Q$  is a good measure of gyrotropy, it is a separate question as to whether it is also useful as a proxy for the identification of reconnection sites. As a first attempt at an answer, we investigate particle-in-cell simulations performed with the code p3d [9]. It employs units based on a field strength  $B_0$  and density  $n_0$ , with lengths normalized to the ion inertial length  $d_i = c/\omega_{pi}$ , where  $\omega_{pi}$  is the ion plasma frequency, and times to the ion cyclotron time  $\Omega_{i0}^{-1}$ .

#### A. Run 1: Anti-Parallel Reconnection

We first consider a variation of the standard GEM Challenge [10]. The simulation domain has dimensions  $(L_x, L_y) = (51.2, 25.6)$  with an initial magnetic field of  $B_x = \tanh(y/w_0)$  and  $w_0 = 0.5$ . There is no initial field component in the  $z$  direction. To ensure pressure balance, the density  $n = n_b + \text{sech}^2(y/w_0)$ , with  $n_b = 0.2$ , and the electron and ion temperatures are initially isotropic with  $T_e = 1/12$  and  $T_i = 5/12$ . The ion-to-electron mass ratio is 400 and the speed of light is 40. The spatial grid has resolution  $\Delta x = 1/160$ , which

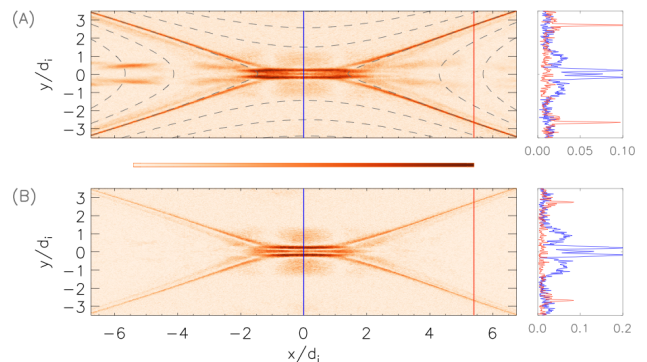


FIG. 1. Images of  $\sqrt{Q}$  (panel A) and  $A\varnothing_e/2$  (panel B) with superimposed magnetic field lines (dotted) for the run described in section III A. Colors represent different values in each image; the central bar shows the relative variation. The data have been averaged over  $0.03\Omega_{ce}^{-1} = 12\Omega_{ce}^{-1}$ , or  $\approx 2$  electron Larmor orbits in the asymptotic field, and over  $0.5d_e$  in each direction. The panels on the right show cuts along the corresponding colored lines in the main images.

means there are 8 gridpoints per electron inertial length ( $d_e$ ) and  $\approx 3$  per electron Larmor radius in the maximum field. There are 100 particles per cell for each species in the asymptotic region.

Figure 1 shows a comparison of  $\sqrt{Q}$  and  $A\varnothing_e/2$  during a time of steady reconnection ( $D_{ng}$  closely follows  $\sqrt{Q}$  in this case and so is not plotted). The magnetic field and pressure tensor components were averaged over  $\approx 2$  electron Larmor orbits and 4 gridpoints ( $0.5d_e$ ) in each direction before computing the gyrotropy measures. Equation A8 was used to calculate  $\sqrt{Q}$ ;  $A\varnothing_e$  was calculated from the formulas given in Appendix A of [6]. In order to minimize subjectivity, no data manipulation (e.g., noise rejection), other than the spatial and temporal averaging, was performed. Only a fraction of the simulation domain is pictured in order to highlight the regions exhibiting strong departures from gyrotropy. On the right-hand side of each image are the traces of two cuts, one through the X-point (blue) and the other  $\approx 5d_i$  downstream (red).

Both  $A\varnothing_e$  and  $Q$  are significant near the X-point, although there are minor differences in the aspect ratio and structural details of the bright regions. The bifurcation at  $y/d_i = 0$  and  $-2 \lesssim x/d_i \lesssim 2$  mirrors that seen in the charge and current densities (not shown) and reflects the complicated dynamics of Speiser particle orbits near the region of null field. The values within a few gridpoints of  $(x, y) = (0, 0)$  carry somewhat more uncertainty because gyrotropy is an ill-defined quantity when  $B = 0$ .

While  $\sqrt{Q}$  and  $A\varnothing_e/2$  both vary between 0 and 1, the more meaningful comparison is between the asymptotic value of each cut, which gives a reasonable approximation of the inherent particle noise, and the peak value at the X-point. These are roughly equal for the two measures. On the other hand, the magnetic separatrices (red peaks) are comparatively much weaker in  $A\varnothing_e$  and stronger in

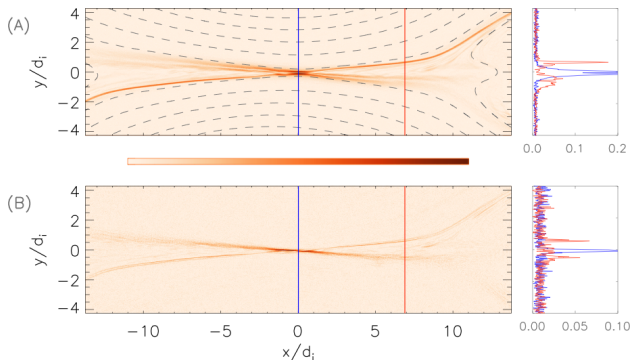


FIG. 2. Images of  $\sqrt{Q}$  (panel A) and  $A\delta_e/2$  (panel B), in the same format as Figure 1, for the run described in section III B. The data have been averaged over  $0.5\Omega_{ci}^{-1} = 12.5\Omega_{ce}^{-1}$ .

$\sqrt{Q}$ . The separatrices mark topological boundaries with, in principle, zero width. If the associated particle signatures exhibit scales near the Larmor radius (as is known to be the case around the X-line) then the intermingling between the upstream and downstream plasmas should produce departures from gyrotropy there.

Both measures show humps just upstream of the X-point that indicate small departures from gyrotropy. These may arise from decreases in  $P_{\perp}$  (due to magnetic moment conservation) followed by scattering to other components. Another possibility is that beams of inflowing electrons, when superimposed on the base Maxwellian, drive the total distribution function away from cylindrical symmetry.

### B. Run 2: Guide-Field Reconnection

As a second case we consider a force-free equilibrium where the initial density ( $n = 1$ ) and temperatures ( $T_i = T_e = 1/8$ ) have no spatial variations. The reconnecting field has the form  $B_x = \tanh(y/w_0)$ , here with  $w_0 = 1$ , but now the out-of-plane (guide) component  $B_z$  varies so that  $B_x^2 + B_z^2$  is constant. The initial guide field is asymptotically 2 and rises to  $\sqrt{5}$  at the current sheet's center. The domain has dimensions  $(L_x, L_y) = (51.2, 25.6)$ , the ion-to-electron mass ratio is 25, and the speed of light is 15. The spatial grid has resolution  $\Delta x = 1/40$ , which implies 8 gridpoints per  $d_e$  and  $\approx 2$  per electron Larmor radius in the maximum field. There are 100 particles per cell for each species.

Figure 2, in the same format as Figure 1, shows the region near the X-point. Both  $\sqrt{Q}$  and  $A\delta_e$  peak there, although again the morphologies in the downstream region exhibit differences. The asymmetry between the separatrices, a common feature of guide-field reconnection, is apparent. As in Figure 1, the cuts show that the separatrices are somewhat stronger in  $\sqrt{Q}$  than in  $A\delta_e$ . In images of the entire domain (not shown), the enhancement of  $\sqrt{Q}$  on the upper-right and lower-left separatrices continues around nearly the entire exterior of the down-

stream magnetic island while  $A\delta_e$  quickly peters out. However, the strongest difference is in the background noise level. While the two measures have similar peak-to-background ratios for the simulation of Section III A, here they differ by a factor of  $\approx 4$ , with  $\sqrt{Q}$  smoother than in Figure 1 and  $A\delta_e$  noisier. The improvement in  $\sqrt{Q}$  can be attributed to the strong guide field and its driving of the plasma towards gyrotropy. The indentation in the magnetic field lines at  $x/d_i \approx 11$  is a transient feature due to the interaction of the outflowing plasma and the remains of a small magnetic island expelled from the X-point earlier in the simulation.

## IV. DISCUSSION

We have proposed a new, mathematically rigorous measure of the gyrotropy of an arbitrary pressure tensor and presented numerical simulations of 2.5D reconnection demonstrating that gyrotropy violations peak near magnetic topological boundaries. Testing the efficacy of  $Q$  in three-dimensional simulations and with spacecraft data are obvious next steps. It is unlikely that any single diagnostic can unfailingly and unambiguously identify reconnection sites in spacecraft data, but  $Q$  offers a complementary approach to methods based on other measurements. The calculation of  $Q$  requires the full electron pressure tensor – available, for instance, on the recently launched Magnetospheric Multiscale Mission – and can be easily performed in any coordinate system using the algorithm presented in Appendix A.

While  $Q$  has some similarities to previously proposed measures, particularly the non-gyrotropy parameter  $D_{ng}$  of [7], there are pressure tensors (e.g., equation 10) for which  $D_{ng}$  does not correctly characterize the gyrotropy. However, in many instances the two give similar results. Their ratio can be written as

$$\frac{Q}{D_{ng}^2} = \frac{(x+2)^2}{8(1+2x)} \quad (12)$$

where  $x = P_{\parallel}/P_{\perp}$ . The right-hand side takes its minimal value for  $x = 1$  and only varies by  $\approx 30\%$  for  $0 \leq x \leq 4$ . Although the ratio can become arbitrarily large when  $x \rightarrow \infty$ , approaching that limit in a real system will trigger other effects. Of particular note is the firehose mode, for which the linear instability criterion is  $\beta_{\perp}(P_{\parallel}/P_{\perp} - 1) > 2$ . Under normal circumstances plasmas cannot significantly exceed this threshold, which thus implies  $x < 1 + 2/\beta_{\perp}$ . As a consequence, the differences between  $D_{ng}$  and  $\sqrt{Q}$  are starkest for  $\beta_{\perp} \ll 1$ . (This argument is strictly only applicable for gyrotropic plasmas because they are assumed in deriving the firehose stability boundary. It should be a reasonable approximation when the pressure tensor is near gyrotropy, but significant off-diagonal components will likely modify the instability threshold.)

The differences between  $Q$  and the agyrotropy  $A\delta_e$  are more significant. The latter only quantifies one type

of departure from gyrotropy, the breaking of cylindrical symmetry in the plane perpendicular to the magnetic field, while the former handles the general case. Of more pressing interest to the interpretation of simulations and observations, however, is how well the measures identify regions of interesting magnetic topology. Both successfully illuminate X-lines for the simulations presented here, but  $Q$  does a better job of tracing magnetic separatrices, particularly in guide-field reconnection. Further analysis is necessary to make these comparisons quantitative.

Finally, an interesting connection exists between  $\mathbb{P}$  and the inertia tensor of a rigid body. Since both are symmetric and positive semi-definite, a measure analogous to  $Q$  also exists for the former. To be relevant, however, something external to the body must define a preferred direction in a manner similar to the role the magnetic field plays in defining gyrotropy.

### ACKNOWLEDGMENTS

We would like to acknowledge helpful conversations with K. Schoeffler. This work was supported by NASA grant NNX14AF42G.

### Appendix A: Calculating $Q$

Beginning with a pressure tensor in an arbitrary coordinate system, the calculation of  $Q$  from equation 6 requires a transformation into a frame in which the diagonal components are in gyrotropic form. A tensor  $\mathbb{A}$  transforms under coordinate rotations according to the prescription

$$\mathbb{A}' = \mathbb{R}^T \mathbb{A} \mathbb{R} \quad (\text{A1})$$

where  $\mathbb{R}$  is a rotation matrix. Both the symmetry of  $\mathbb{A}$  and its eigenvalues are preserved after rotation of the coordinate axes.

As an example, we demonstrate that, beginning with a pressure tensor of the form

$$\mathbb{P} = \begin{pmatrix} P_{\parallel} & P_a & P_b \\ P_a & P_{\perp 1} & P_c \\ P_b & P_c & P_{\perp 2} \end{pmatrix}, \quad (\text{A2})$$

it is always possible to find a coordinate system in which the final two diagonal entries are equal. To do so, rotate around the magnetic field direction with the rotation matrix

$$\mathbb{R} = \begin{pmatrix} 1 & 0 & 0 \\ 0 & \cos \theta & -\sin \theta \\ 0 & \sin \theta & \cos \theta \end{pmatrix}. \quad (\text{A3})$$

Calculating  $\mathbb{R}^T \mathbb{P} \mathbb{R}$  and setting the second and third diagonal components equal gives the required angle:

$$\tan(2\theta) = \frac{P_{\perp 2} - P_{\perp 1}}{2P_c}. \quad (\text{A4})$$

In the new frame the final two diagonal components are  $(P_{\perp 1} + P_{\perp 2})/2$ . The off-diagonal elements must also be known in the new coordinate system in order to compute  $Q$ . Although explicit expressions for them can be calculated, the algebra is somewhat tedious.

An easier method relies on the fact that certain combinations of tensor elements are invariant under coordinate rotations. Through their use,  $Q$  can be computed when  $\mathbb{P}$  is known in any coordinate system. In particular, a  $3 \times 3$  tensor with elements  $P_{ij}$  in an arbitrary Cartesian system with coordinates  $(x, y, z)$  has three invariants, two of which are the trace

$$I_1 = P_{xx} + P_{yy} + P_{zz} \quad (\text{A5})$$

and the sum of principal minors

$$I_2 = P_{xx}P_{yy} + P_{xx}P_{zz} + P_{yy}P_{zz} - (P_{xy}P_{yx} + P_{xz}P_{zx} + P_{yz}P_{zy}). \quad (\text{A6})$$

For symmetric matrices  $P_{ij} = P_{ji}$  and the final three terms of  $I_2$  simplify. The third invariant, not used here, is the determinant.

With these definitions  $Q$  can be expressed in terms of  $I_1$ ,  $I_2$ , and the parallel pressure  $P_{\parallel}$ . The latter can be calculated from

$$P_{\parallel} = \hat{\mathbf{b}} \cdot \mathbb{P} \cdot \hat{\mathbf{b}} = b_x^2 P_{xx} + b_y^2 P_{yy} + b_z^2 P_{zz} + 2(b_x b_y P_{xy} + b_x b_z P_{xz} + b_y b_z P_{yz}) \quad (\text{A7})$$

where  $b_i$  is the  $i^{\text{th}}$  component of the unit vector aligned with the local magnetic field. After some algebraic manipulations,

$$Q = 1 - \frac{4I_2}{(I_1 - P_{\parallel})(I_1 + 3P_{\parallel})}. \quad (\text{A8})$$

With this formula  $Q$  can be simply computed in an arbitrarily oriented coordinate system, without need for coordinate transformations and the associated matrix multiplications.

[1] K. Schindler, M. Hesse, and J. Birn, *J. Geophys. Res.* **93**, 5547 (1988).

[2] J. C. Dorelli and A. Bhattacharjee, *Phys. Plasmas* **15**,

- 056504 (2008).
- [3] A. L. Haynes and C. E. Parnell, *Phys. Plasmas* **17**, 092903 (2010).
  - [4] C. M. Komar, P. A. Cassak, J. C. Dorelli, A. Glozer, and M. M. Kuznetsova, *J. Geophys. Res.* **118**, 4998 (2013).
  - [5] V. M. Vasyliunas, *Rev. Geophys.* **13**, 303 (1975).
  - [6] J. Scudder and W. Daughton, *J. Geophys. Res.* **113**, A06222 (2008).
  - [7] N. Aunai, M. Hesse, and M. Kuznetsova, *Phys. Plasmas* **20**, 092903 (2013).
  - [8] R. A. Horn and C. R. Johnson, *Matrix Analysis* (Cambridge University Press, 2012), chap. 7, pp. 429–439, ISBN 9780521839402.
  - [9] A. Zeiler, D. Biskamp, J. F. Drake, B. N. Rogers, M. A. Shay, and M. Scholer, *J. Geophys. Res.* **107**, 1230 (2002).
  - [10] J. Birn, J. F. Drake, M. A. Shay, B. N. Rogers, R. E. Denton, M. Hesse, M. Kuznetsova, Z. W. Ma, A. Bhattacharjee, A. Otto, et al., *J. Geophys. Res.* **106**, 3715 (2001).